Elsevier has created a Monkeypox Information Center in response to the declared public health emergency of international concern, with free information in English on the monkeypox virus. The Monkeypox Information Center is hosted on Elsevier Connect, the company's public news and information website.

Elsevier hereby grants permission to make all its monkeypox related research that is available on the Monkeypox Information Center - including this research content - immediately available in publicly funded repositories, with rights for unrestricted research re-use and analyses in any form or by any means with acknowledgement of the original source. These permissions are granted for free by Elsevier for as long as the Monkeypox Information Center remains active.

Journal of Infection and Public Health 16 (2023) 996–1003

Contents lists available at ScienceDirect

Journal of Infection and Public Health

journal homepage: www.elsevier.com/locate/jiph

Original article

Exploration of natural compounds against the human mpox virus DNA-dependent RNA polymerase *in silico*

Jameel M. Abduljalil [a], Abdo A. Elfiky [b,*], Alaa M. Elgohary [b]

[a] Department of Biological Sciences, Faculty of Applied Sciences, Thamar University, Dhamar, Yemen
[b] Biophysics Department, Faculty of Science, Cairo University, Giza, Egypt

ARTICLE INFO

Article history:
Received 18 January 2023
Received in revised form 18 April 2023
Accepted 27 April 2023

Keywords:
Mpox
DdRp
Natural compounds
Molecular dynamics simulation
Infectious diseases

ABSTRACT

Background: Last year, the human monkeypox virus (hMPXV) emerged as an alarming threat to the community, with a detectable outbreak outside the African continent for the first time. According to The American Centers for Disease Control and Prevention (CDC), the virus is reported globally, with 86,746 confirmed cases (until April 08, 2023). DNA-dependent RNA polymerase (DdRp) is an essential protein for viral replication; hence it is a promising drug target for developing antiviral drugs against DNA viruses. Therefore, this study was conducted to search for natural compounds that could provide scaffolds for RNA polymerase inhibitors.

Methods: In this study, the DdRp structure of hMPXV was modeled and used to screen the natural compounds database (COCONUT). The virtual screening revealed 15 compounds able to tightly bind to the active site of the DdRp (binding energies less than −7.0 kcal/mol) compared to the physiological nucleotide, guanosine triphosphate (GTP). Molecular dynamics simulation was then performed on the top four hits and compared to GTP

Results: The results revealed the potential of four compounds (comp289, comp295, comp441, and comp449) in binding the hMPXV DdRp active site with a comparable binding affinity (−17.06 ± 2.96, −11.6 ± 5.34, −14.85 ± 2.66, and −10.79 ± 4.49 kcal/mol) with GTP (−21.03 ± 7.55 kcal/mol)

Conclusion: These findings may also pave the way for developing new hMPXV inhibitors based on natural product scaffolds. These results need further experimental validation but promising as it was validated by unbiased all-atom MD simulations and binding free energy calculations.

1. Introduction

Human monkeypox virus (hMPXV) is a recently emerged double-stranded DNA virus that belongs to the *Orthopoxvirus* genus in the *Poxviridae* family. This taxon harbors several zoonotic or human-specific agents, such as the smallpox virus, cowpox virus, camelpox virus, and molluscum contagiosum virus [1]. The virions of *Poxviridae* are characterized by their complex brick-shaped structure (200–400 nm) in which viral genomes, and other essential proteins, are contained in a dumbbell-shaped core structure between two lateral bodies [1]. The genomes of poxviruses are exceptionally large, encoding more than a hundred proteins involved in viral structure, replication, virulence, and immuno-modulators to counteract the immune response mounted by the infected host [2].

Until 2020, small-scale outbreaks occurred in Africa, and viral transmission was limited in terms of location and cases; less than 700 cases per event [3]. The infections were usually linked to direct contact with wild animals like squirrels and monkeys. However, its natural reservoir is still unidentified. A single outbreak outside the African continent was reported in the USA in 2003 producing 71 human infections [4]. Since 2017, sporadic cases have been reported outside the endemic African regions [5]. The ongoing outbreak of hMPXV started in May 2022 as a cluster of cases in the UK, and the index case was identified as a traveler from Nigeria; however, the exact time for the spread of the virus is still unknown. According to the American CDC surveillance, the virus is spreading globally in regions that have not historically reported Monkeypox infections, with 86,746 confirmed cases (until April 08 2023) [6]. Body fluids, contaminated items, physical contact with infected individuals, and respiratory droplets are believed to be the main routes of the ongoing transmission chains [7].

* Corresponding author.
E-mail address: dr_abdo@cu.edu.eg (A.A. Elfiky).

https://doi.org/10.1016/j.jiph.2023.04.019

Clinically, hMPXV has a milder virulence than the smallpox virus, with a case fatality rate of 3–6 % [2]. The infection manifests 1 – 3 weeks after exposure to the virus as non-specific symptoms such as fever and muscle pain. Lymphadenopathy accompanies skin rash that develops into blisters and crusts that occur in 1–3 days after the appearance of a fever [8]. The symptoms remain 2–4 weeks before resolution; other cases may be asymptomatic or with previously unreported symptoms. The infection is usually self-limited but severe, and a bad prognosis was seen in immunocompromised individuals [2,8]. After viral entry by direct fusion with cell membranes or micropinocytosis, poxviruses replicate in the cytoplasm, and early-stage genes are expressed to produce essential proteins for viral replication and modulation of the immune response [2,8]. Tecovirimat is the first drug being approved for poxviruses that limit the infection by inhibiting viral egress from infected cells [9]. However, it is still widely unavailable.

Transcription factors, DNA and RNA polymerases, capping enzymes, and methylases are all early-stage proteins required for viral genome replication [8]. The DNA-dependent RNA polymerase (DdRp) of poxvirus is a multi-chain complex that resembles its eukaryotic counterpart, especially the RNA polymerase of yeast [10]. DdRp is responsible for poxviral replication in the host cell's cytoplasm without the need to enter the nucleus as other DNA viruses [2]. Unfortunately, all the approved antiviral drugs to treat double-stranded DNA viruses are inhibitors of either the DNA polymerase or the reverse transcriptases [11]. However, no approved or experimental compounds are reported to inhibit RNA transcription in poxviruses. Therefore, it is a promising drug target for developing new chemotherapeutic antiviral drugs against DNA viruses. Cidofovir (cytidine analog) is another anti-poxvirus drug given topically or by injections. Nonetheless, nephrotoxicity is a major side effect and a dose-limiting factor for cidofovir [12]. Therefore, in this study, we virtually screened the natural compounds database COCONUT (COlleCtion of Open Natural prodUcTs) [13] against the DdRp aiming to find potential leads as DdRp inhibitors.

2. Materials and methods

2.1. Modeling and simulation dynamics of DdRp

In this study, we used the model of hMPXV DdRp, as reported previously [14]. The amino acid sequence of hMPXV DdRp chain A was obtained from the NCBI database (GenBank: AAY97089.1). A BLAST search against PDB entries identified several structures of Vaccinia virus DdRp as the best homologs with a sequence identity of 99.22 % and 100 % coverage. The model was assembled using the SWISS-MODEL web server from the Vaccinia virus elongation complex structure (PDB ID: 6RID). The model was valid based on the MolProbity server of Duke University [15]. The active site's metal ion (Mg^{2+}) was added based on the coordination seen in the template model. Side chains of active site residues were modified via the

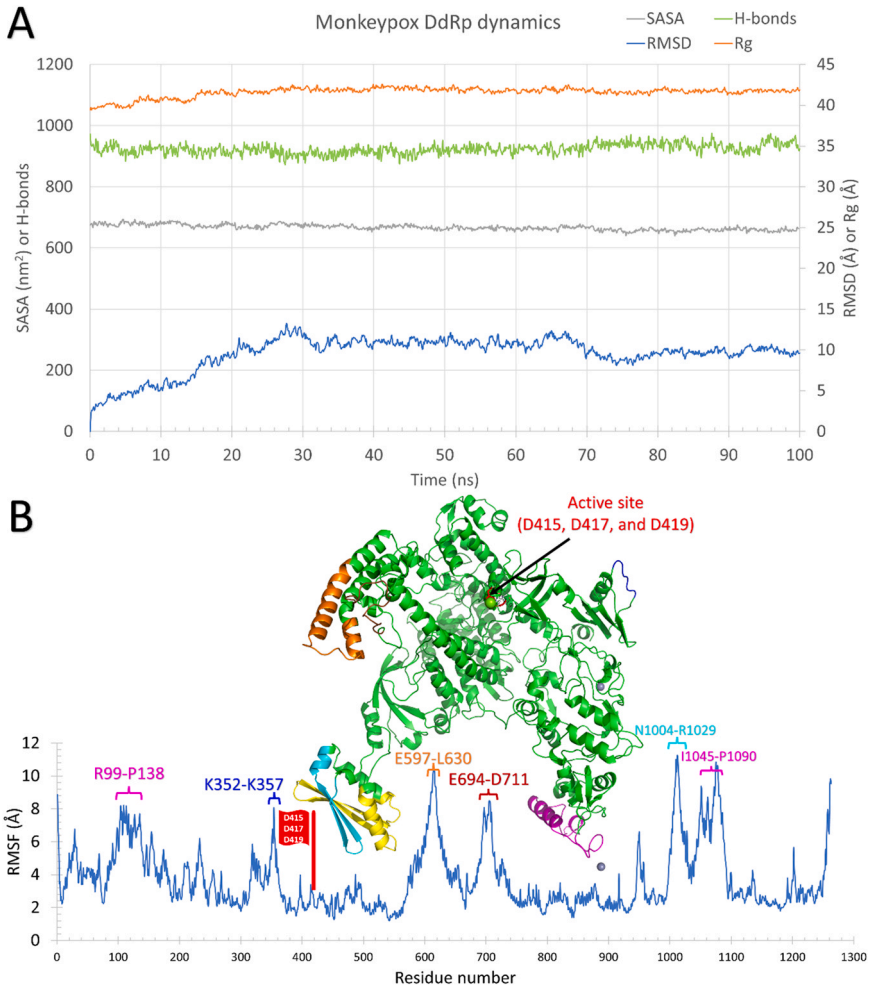

Fig. 1. The molecular dynamics simulation analysis of the Apo DdRp. (A) Protein behavior analyses (B) The per-residue root-mean-square fluctuations (blue curve) with the DdRp structure taken at 50.9 ns during the MD simulation represented by the colored cartoon (top). The high fluctuating regions (RMSF < 6 Å) during the MD simulation were shown by different colors on the RMSF curve and the structure. The active sites (D415, D417, and D419) are also shown in red.

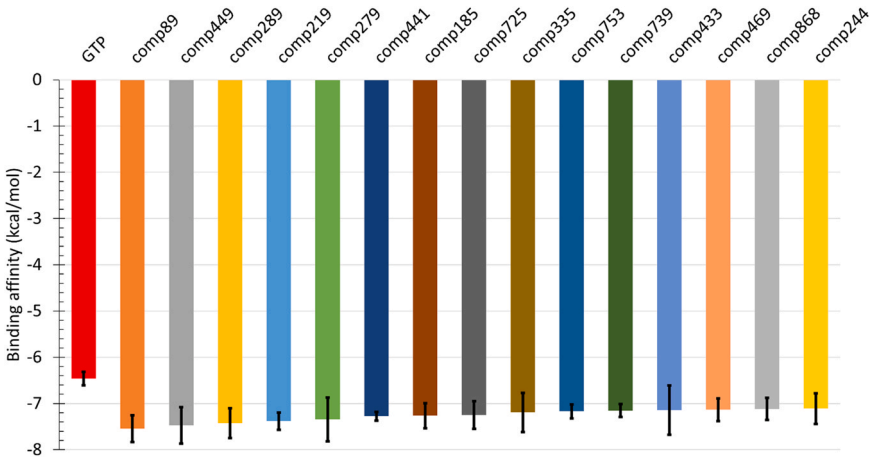

Fig. 2. Average calculated binding energies of the top 15 compounds along with the physiological substrates (guanosine triphosphate (GTP) (red column). Error bars represent the standard deviation of binding affinity (kcal/mol) of three clusters representative conformations of the protein after MD simulation.

Dunbrack library in UCSF Chimera to achieve the required coordination geometry [16,17].

2.2. MD simulation

The model of DdRp was subjected to molecular dynamics (MD) simulation using GROMACS 2021 package [18] and CHARMM36 forcefield. The system was prepared via CHARMM-GUI by model solvation in physiological conditions (0.15 M) of Na^+ and Cl^- ions and TIP3P water model [19]. The steepest descent algorithm minimized the system energy for 50,000 steps. Next, an ensemble of constant number, volume, and temperature (NVT) was applied to equilibrate the system for two ns, where the temperature was coupled by the Berendsen thermostat [20]. A subsequent system equilibration was performed using the constant number, pressure, and temperature (NPT) ensemble for additional two ns. Parrinello-Rahman and velocity-rescaling algorithms controlled the pressure and temperature [21,22]. Periodic boundary conditions were applied, and the LINC algorithm positionally restrained atoms containing hydrogen. The production run was done in the NPT ensemble for 100 ns without any positional restraints. Post-dynamic analyses were performed using the built-in modules in GROMACS. Finally, the trajectory was clustered by TTClust [23] to obtain multiple conformers of the DdRp at different dynamics states.

2.3. DdRp and compounds preparation

The representative conformers obtained from the clustering of the simulation trajectory were protonated at a pH of 7.4 by the H+ + server [24] and prepared with AutoDock tools [25]. On the other hand, The COCONUT database [13] of natural product compounds (~0.9 M compounds) was downloaded in the SMILES format and filtered according to the rule-of-five that, resulted in 220 k compounds. DeepPurpose library [26] of drug-target interaction prediction – based on a deep learning approach– was used to estimate the binding of the molecules to the DdRp of the HMPXV. The model pre-trained on the BindingDB, and convolutional neural networks (CNN models) as encoders for the molecules and protein were used in their default parameters. A total of 1174 compounds were predicted to have pK_d of ≤ 5 nM and were chosen for molecular docking. The 3D conformers for the selected molecules were generated by RDkit [27], energetically minimized using the universal force field, and protonated at a pH of 7.4 via OpenBabel [28].

2.4. Molecular docking

Using the three conformers of the DdRp, AutoDock Vina [29] was used for a quick molecular docking of the prepared compounds in a grid box of 30 × 30 × 30 Å centered at the active site (Asp415, Asp417, and Asp419). All compounds with a docking score ≤ – 8 kcal/mol were subjected to the second run of molecular docking in which active site residues were made flexible and the exhaustiveness was increased to 200 to account for the high torsions of the ligands [30].

2.5. MD simulation of top hits and binding free energy calculations

The top four hits in the complex with the hMPXV DdRp were subjected to 100 ns MD simulation using GROMACS 2021 to verify their binding stability to the active site. GTP was also simulated as a positive control in this study. Topologies of the compounds were

Table 1
The established interactions upon docking the top 4 compounds and the physiological ribonucleotides (GTP) against hMPXV DdRp after dynamics.

Compound# (Coconut ID) Generic name	Hydrophobic interactions n	Residues	Hydrogen bonds n	Residues	Salt bridge n	Residues
GTP			8	R380, Q381, L384, H385, **D415**, W422, and R757	3	R380
Comp441 (CNP0267280) **Salpichrolide J**	6	W209, I210, K282, R287, Y306, and W422	3	K282 and R287		
Comp449 (CNP0082649) **20-Hydroxytubocapsanolide A**	-	-	3	N388, S750, and G753		
Comp289 (CNP0158693) **NA**	3	L384	2	N388 and S750		
Comp295 (CNP0350754) **Anabsinthin**	3	R380, L384, and N413	1	N388	2	R380 and H385

Active site residues are in bold. NA: no generic name is available.

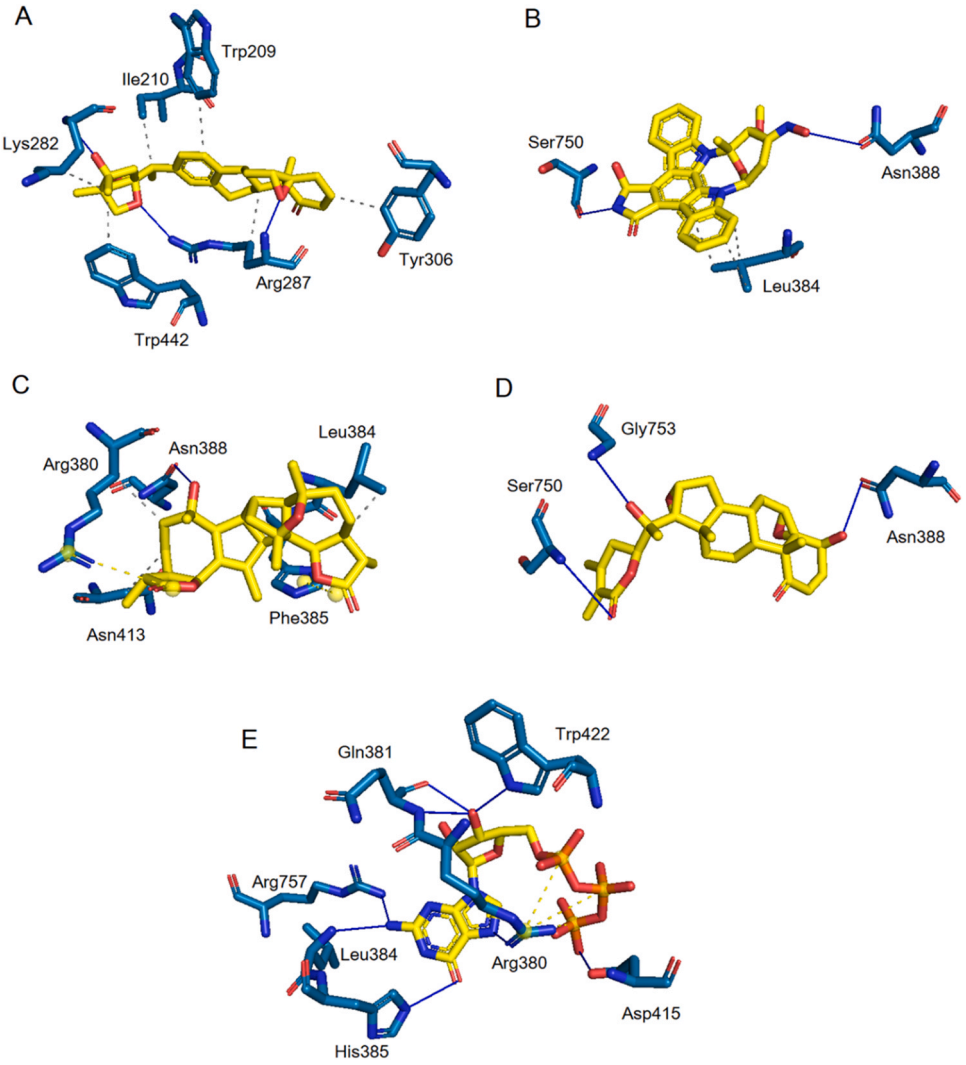

Fig. 3. Post-docking 3D representations of established interactions between natural compounds and residues near the active site of the DdRp. (A) Comp441, (B) Comp289, (C) Comp295, (D) Comp449, and (E) GTP. Bond types are color-coded: H-bonds; blue lines, hydrophobic interactions; dashed-gray lines, and salt bridge; dashed-yellow lines.

obtained from the CGenFF server [31] during systems preparation using CHARMM-GUI [19]. At the same time, the other parameters of the simulation were identical to that used for the apo hMPXV DdRp simulation mentioned before. After that, the molecular mechanics-generalized Born surface area (MM-GBSA) calculations were performed for the four hits-DdRp and GTP-DdRp complexes. The gmx_MMPBSA program [32] was utilized to estimate the binding free energy of potential drugs through calculations of molecular mechanics/generalized-Born surface area [33]. Finally, the last 50 ns of the simulation were used to estimate binding free energy using the second model [34] implemented in MMPBSA.py (gb = 5) [35].

3. Results

3.1. The DdRp model of hMPXV

The predicted model has good quality as judged by Molprobity analysis (Table S1). Only 0.4 % of residues (five) have phi or psi angles in the generously allowed region and no outliers in the Ramachandran plot (Fig. S1). In hMPXV, the active site (D415, D417, and D419) was predicted in the Rpo147 chain at a β-turn between two helices.

3.2. MD simulation of apo DdRp

The structure of the Apo DdRp was subjected to a 100 ns MD simulation run aiming to equilibrate the system and visit the available conformations of the protein during this time. Fig. 1 shows MD simulation analysis parameters calculated from the trajectories using GROMACS built-in modules and in-house tools. As reflected from the curves, the system was equilibrated after 30 ns of the simulation, where the root-mean-square deviation (RMSD) curve is flattened with an average value after equilibration of 10.36 Å. Additionally, the Rg and SASA values are stable during the simulation period, with average values of 41.84 Å and 663.67 nm^2, respectively.

The per-residue root-mean-square fluctuations (RMSF) in Å are shown in Fig. 1B. The structure of DdRp is represented in the colored cartoon (top) to resemble the highly fluctuating (flexible) regions (RMSF < 6 Å) with different colors. In addition to the N- and C-terminals of the proteins, six flexible regions are identified; R99-P138 (magenta), K352-K357 (blue), E597-L630 (orange), E694-D711 (brown), N1004-R1029 (cyan), and I1045-P1090 (yellow). All these highly flexible regions lie apart from the active site (D415, D417, and D419), which is shown in red sticks (RMSF > 3 Å). This suggests the stability of the active site and its usefulness as a drug target.

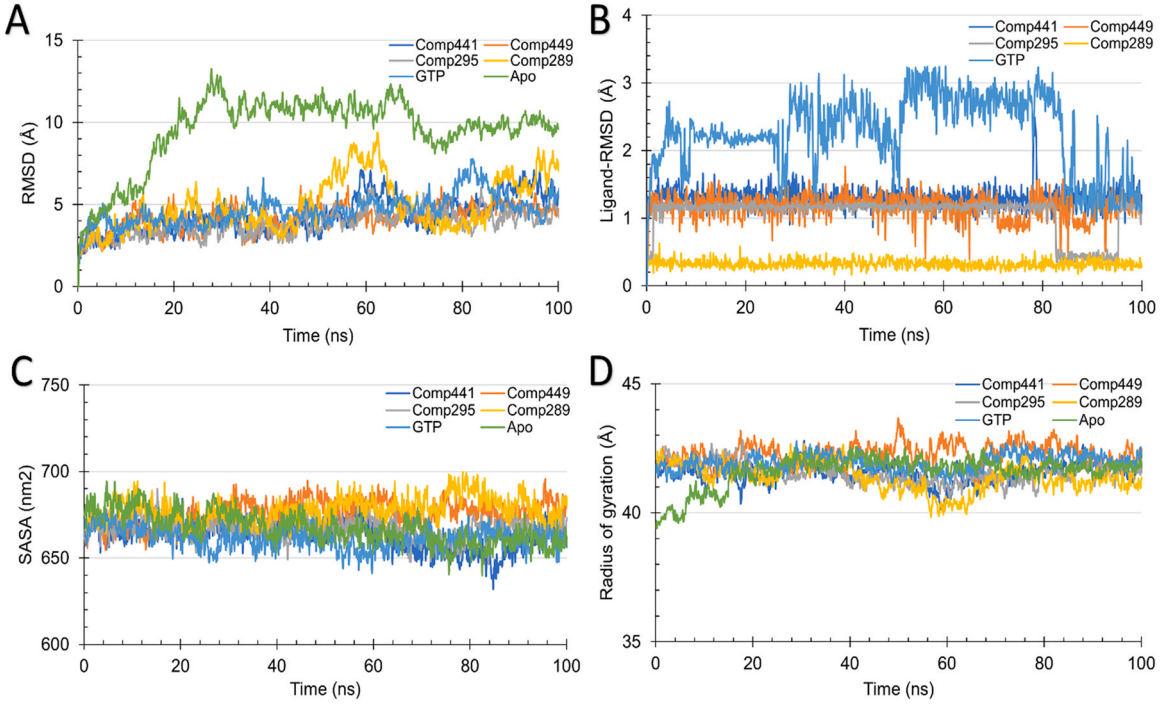

Fig. 4. MD simulation analyses of DdRp behavior and the selected hits. (A) Protein backbone RMSD, (B) ligands RMSD, (C) SASA in nm2, and (D) the radius of gyration.

3.3. Virtual screening by molecular docking

The average binding affinities of the best 56 natural compounds (by flexible docking) against the hMPXV DdRp active site ranged from − 5.76 ± 1.89 to − 7.54 ± 0.29 kcal/mol. The average scores of the top 15 compounds and GTP (red column) are depicted graphically in Fig. 2**.** As the bar graph reflects, all 15 compounds bind better to the protein near the active site than the positive control, with average binding affinities of > −7.11 kcal/mol.

The detailed interactions established upon docking for some selected top hits (binding affinity > −7.0 kcal/mol) are listed in Table 1. Different interaction patterns are observed; for GTP and 20-Hydroxytubocapsanolide A (Comp449), mainly H-bonds are formed and contribute to the binding. On the other hand, in Salpichrolide J, Anabsinthin, and Comp289, both H-bonds and hydrophobic contacts are formed. GTP and Anabsinthin also formed salt bridges to nearby arginine and histidine residues (R380 and H385). The active site residues (D415, D417, and D419) are bolded in Table 1. The interactions are graphically depicted in Fig. 3 (A-E), where the formed interactions are shown by blue lines (H-bonds), dashed-gray lines (hydrophobic contacts), and dashed-yellow lines (salt bridges). Cyan sticks show the interacting residues of the DdRp, whereas the yellow sticks are the ligands. The residues involved in contact with the natural products are scattered in the cavity of the DdRp near the active site.

3.4. Pharmacokinetic and medicinal properties

The predicted absorption, distribution, metabolism, and excretion-toxicity (ADMET) properties of the top four compounds are summarized in Table S2. The four compounds were predicted to be either moderate or totally water soluble, with a high probability of being absorbable in the human gastrointestinal tract. Except for Comp295, the compounds are predicted to have a good volume of distribution (> 1 L/kg), clearance rate (19.82–20.60 ml/min/kg), and absence or moderate toxicity according to Ames toxicity drug-induced liver injury predictive models.

3.5. MD simulation of top analogs

We performed another round of MD simulation for the best four hits Salpichrolide J, Anabsinthin, 20-Hydroxytubocapsanolide A, and Comp289, along with the positive control, GTP, to study the protein dynamics upon ligand binding. Fig. 4 shows the analysis of the DdRp-ligands dynamics for 100 ns simulation per system. As reflected from the flattened RMSD curves, all the systems are equilibrated during the first 30 ns of the simulation with varying RMSD after equilibration. The Apo DdRp shows higher RMSD (around 10 Å) values than the complexes (about 5 Å). This reflects the stability imposed for DdRp upon ligand binding. Comp289-DdRp complex shows fluctuating RMSD during the simulation (between 3 and 8 Å). This complex also shows slightly higher SASA values compared to other complexes.

Different trends are present regarding the ligand RMSD curves (Fig. 4B). Except for the complex of GTP-DdRp (cyan), all the complexes show stable RMSD (> 1.5 Å), while for GTP-DdRp, the ligand-RMSD values are high up to 3.2 Å. This indicates that GTP-DdRp had high mobility during the simulation period, which was also reflected by the high number of formed H-bonds between the ligand and the protein during the course of the simulation (Fig. 5B). The triphosphate moiety is likely the main factor for the higher number of hydrogen bonds formed by the GTP. In addition, the radius of gyration and SASA are stable during the simulation for all complexes (around 42 Å and 660 nm^2, respectively).

The per-residue root-mean-square fluctuations (RMSF) curves of the complexes are presented in Fig. 5C. Again the active site residues (D415, D417, and D419) are stable in all complexes and show RMSF > 4 Å (marked by the red flag). The same six regions in the apo DdRp (Fig. 1B) also have high values of RMSF in all the complexes (RMSF < 5 Å). Additionally, two regions of lower fluctuations for the complexes compared to the apo DdRp are found in the RMSF curve.

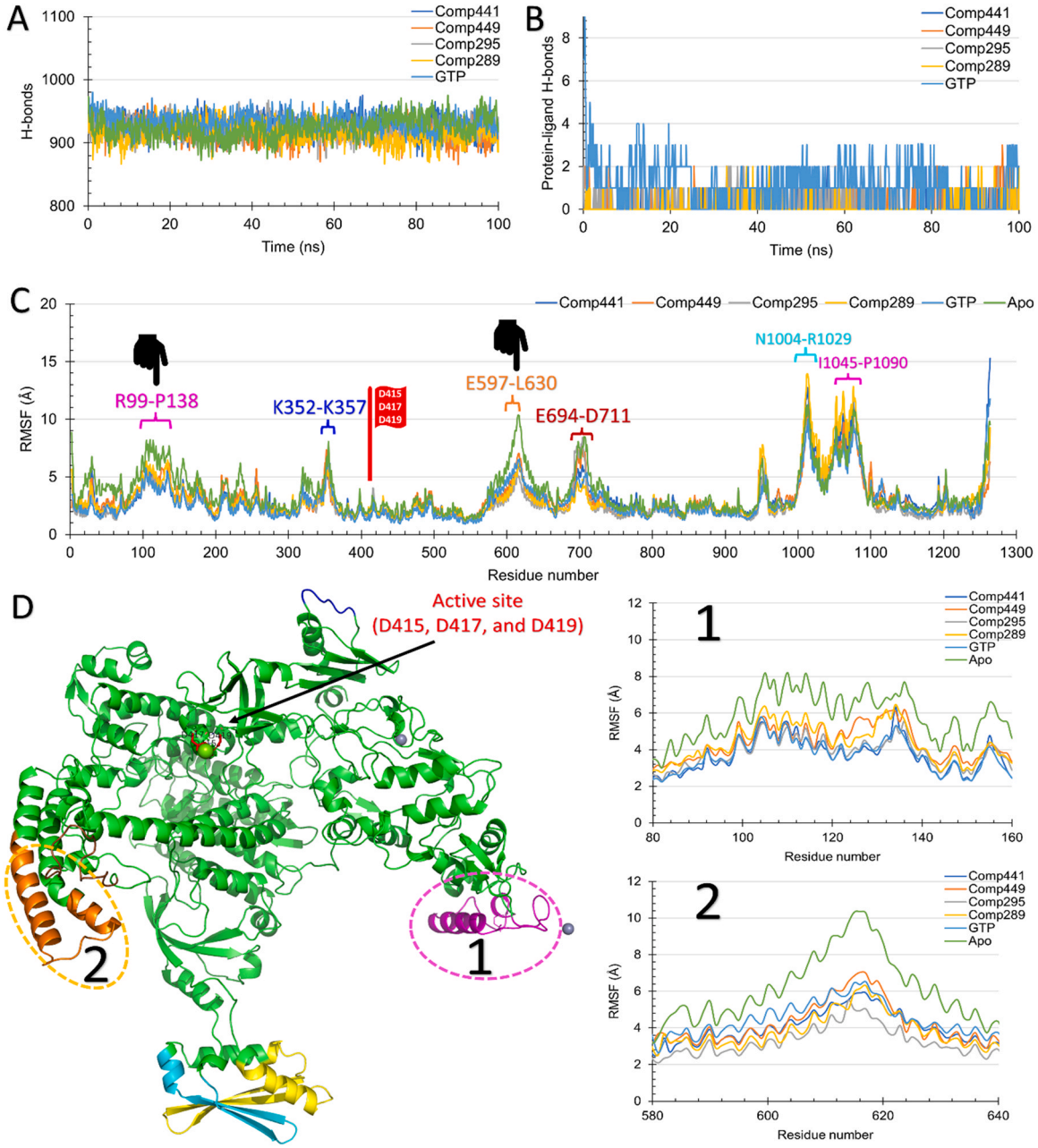

Fig. 5. The molecular dynamics simulation analysis of the top four hits against hMPXV DdRp. (A) the total number of formed H-bonds, (B) protein-ligands formed H-bonds, versus the simulation time in ns for the four top hit complexes, the positive control (GTP), and the Apo form. (C) the per-residue root-mean-square fluctuations in Å are also shown for the same complexes. Highly fluctuating regions are indicated by different colors, while regions of reduced fluctuation compared to the apo DdRp are marked on the RMSF curve. (D) the two regions of reduced RMSF in the complexes compared to the apo DdRp are enlarged (right) and shown in the structure (left).

These regions are plotted in Fig. 5D (right) and marked in the structure (left side). These include; R99-P138 (magenta) and E597-L630 (orange). The reduced fluctuations in these regions reflect its stability upon ligand binding to the DdRp.

3.6. MM/GBSA of the top analogs

Fig. 6 shows the calculated MM/GBSA of the top four complexes (comp441 (blue), comp289 (orange), comp295 (gray), and comp449 (yellow)) and the GTP-DdRp complex (red). Comp289 and comp441 are the best two compounds in binding hMPXV DdRp with values (−17.06 ± 2.96 and −14.85 ± 2.66 kcal/mol) compared to the positive control (GTP) (−21.03 ± 7.55 kcal/mol).

4. Discussion

The DdRp in poxviruses is a large multisubunit structure that requires transcription factors to initiate and terminate the transcription of viral genes [36]. The eight subunits of the transcription complex are named according to their molecular weights: Rpo174, Rpo132, Rpo35, Rpo30, Rpo22, Rpo19, Rpo18, and Rpo9. The former two chains share 20 % of their amino acid sequences with the host RNA polymerase II [37]. These two chains are also assembled in a bilobal structure where the active site is held in a cleft between the subunits.

Since smallpox was the only human infection of medical significance that has been eradicated through vaccination, limited research has been conducted on identifying anti-poxvirus drugs. Based

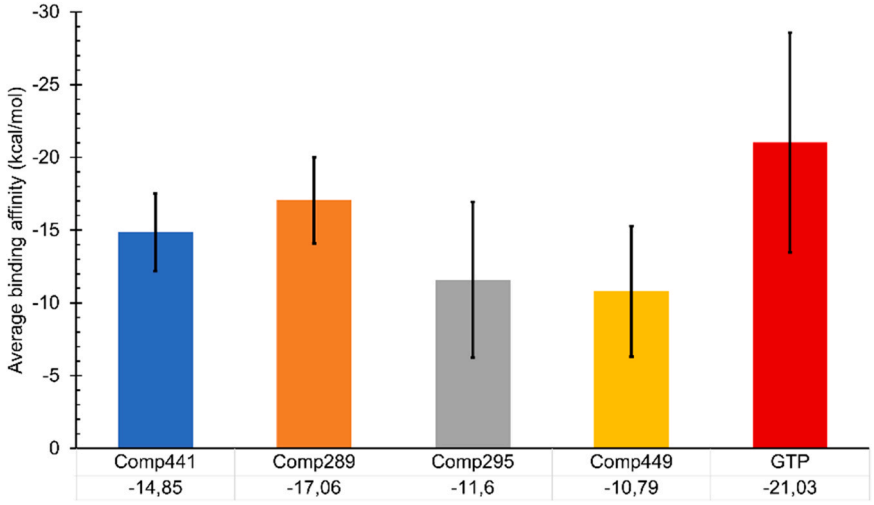

Fig. 6. The calculated MM/GBSA for the positive control (GTP) and the best four ligands (comp441, comp289, comp295, and comp449)-hMPXV DdRp. The error bars represent the standard deviation.

on our previous results [14], the top 15 natural products from the docking step show lower binding energies (i.e., higher affinities to the DdRp) than the four nucleotide triphosphates, which may indicate promising scaffolds for non-nucleoside inhibitors as seen in other compounds from natural sources [38,39]. The interaction of identified compounds with R380 and H385, and the nearby amino acids, is interesting since counterpart residues in the actively transcribing model of the vaccinia virus (PDB: 6RID) are involved in direct contact with the backbone of the DNA strand being transcribed. Occupying such a region with a strong binder molecule is expected to impair the viral DNA transcription process.

Withanolides are a wide group of active natural steroid compounds built on the C28 ergostane skeleton, predominantly isolated from several genera of the *Solanaceae* family. The common characteristics of most withanolides are the oxidation of C-22 and C-26 to form the δ-lactone ring. Modifications on the steroid nucleus and the side chain are the main features of the biotransformed compounds. Withanolides are a group of naturally occurring C28-steroidal lactones built on an intact or rearranged ergostane framework. Withaferin A is the first member of withanolides to be isolated and is the most abundant withanolide present in *Withania somnifera*. Different bioactivities have been assigned to Withanolides, including antibacterial, anti-inflammatory, and anticancer functions by inhibiting mitosis and cytoskeletal changes that would enable growth and malignancy [40,41]. Tettamanzi isolated Salpichrolide J from the leaves of *Salpichroa origanifolia* found in northwest Argentina. However, there is no available pharmacological data on this withanolide [42]. Additionally, 20-HydroxytubocapsanolideA is one of the withanolides isolated from *Tubocapsicum anomalum* roots using (bioassay-directed fractionation). It is the hydroxy derivative of tubocapsanolide A. It shows a remarkable cytotoxic effect against different human cancer cell lines, including hepatocellular, breast, and lung carcinomas, in addition to the embryonic lung cell line MRC-5.

The p-sec-amyl phenol (Anabsinthin) is one of the natural compounds (sesterterpenoids), sesquiterpenoid lactones, with proven medicinal efficiency. Sesterterpenoids are a branch of the terpenoid family. They are a small group of natural products isolated from a wide range of organisms, including microorganisms, plants, marine organisms, and some insects. Anabsinthin considers a strong bitter agent, along with absinthin in the wormwood plant (*Artemisia absinthium*). The Wormwood plant is known for its wide applications in traditional medicine and the biological activity of its extracts [43].

Lastly, end-point free energy calculations have proved their usefulness in correctly predicting the binding pose and ranking the hits from docking-based virtual screening [33]. The two compounds form stable complexes with DdRp active sites that possess good binding affinities and hence are suggested as potential leads against hMPXV DdRp. Further analysis by in vitro and in vivo assays is recommended.

5. Conclusion

Computational drug design succeeded in finding new inhibitors or repurposing drugs for recent viral outbreaks. We modeled the DdRp of the human monkeypox virus (hMPXV) using homology modeling followed by virtual screening of +0.9 M natural compounds-based drugs using combined artificial intelligence and molecular docking. MD simulation was then performed on the apo DdRp and the docked complexes (best four compounds), followed by MM/GBSA calculations. In the current study, we report the potential inhibitory activity of two compounds (Comp289 and comp441) against the hMPXV. Based on our docking results, dynamics simulations, and calculated binding energies, we suggest experimental validation and/or lead optimization of these two natural compounds against the DdRp of hMPXV. This could help in fighting against the current outbreak that spread worldwide.

Funding

This work is based upon work supported by Science, Technology and Innovation Funding Authority (STDF) under the grant number 45696.

Ethical statement

No data was generated from human subjects or animals. Not required as no humans or animals are involved in this work.

CRediT authorship contribution statement

J.M.A. performed the calculations and wrote the first draft. **A.M.E.** wrote the manuscript and discussion, while **A.A.E.** revised the study design, supervised the study, made figures, and contributed to discussions and proofreading of the final manuscript.

Declaration of Competing Interest

The authors have declared no conflict of interest.

Acknowledgments

We are thankful to Bibliotheca Alexandrina for providing access to their High-Performance Computing facility.

Appendix A. Supporting information

Supplementary data associated with this article can be found in the online version at doi:10.1016/j.jiph.2023.04.019.

References

[1] Moss B. Poxviridae. In: Knipe DM, Howley PM, editors. Fields Virology. sixth ed.Philadelphia, USA: Lippincott Williams & Wilkins; 2013. p. 2129–59.
[2] Damon IK. Poxviruses. In: Knipe DM, Howley PM, editors. Fields Virology. sixth ed.Philadelphia, USA: Lippincott Williams & Wilkins; 2013. p. 2160–84.
[3] Meyer H, Perrichot M, Stemmler M, Emmerich P, Schmitz H, Varaine F, et al. Outbreaks of disease suspected of being due to human monkeypox virus infection in the democratic Republic of Congo in 2001. J Clin Microbiol 2002;40:2919–21. https://doi.org/10.1128/JCM.40.8.2919-2921.2002
[4] Reed KD, Melski JW, Beth Graham M, Regnery RL, Sotir MJ, Wegner MV, et al. The detection of Monkeypox in humans in the western hemisphere. N Engl J Med 2004;350:342–50. https://doi.org/10.1056/NEJMOA032299
[5] Beer EM, Bhargavi Rao V. A systematic review of the epidemiology of human monkeypox outbreaks and implications for outbreak strategy. PLOS Negl Trop Dis 2019;13:e0007791. https://doi.org/10.1371/JOURNAL.PNTD.0007791
[6] The Centers for Disease Control and Prevention. 2022 Mpox Outbreak Global Map 2023. https://www.cdc.gov/poxvirus/mpox/response/2022/world-map.html (accessed April 14, 2023).
[7] Bunge EM, Hoet B, Chen L, Lienert F, Weidenthaler H, Baer LR, et al. The changing epidemiology of human monkeypox – a potential threat? A systematic review. PLOS Negl Trop Dis 2022;16:e0010141. https://doi.org/10.1371/JOURNAL.PNTD.0010141
[8] Isaacs SN, Buller RM. Poxviruses Clin Virol 2016:385–413. https://doi.org/10.1128/9781555819439.CH19
[9] Rizk JG, Lippi G, Brandon ·, Henry M, Forthal DN, Rizk Y. Prevention and treatment of monkeypox. Drugs 2022:1–7. https://doi.org/10.1007/S40265-022-01742-Y
[10] Mirzakhanyan Y, Gershon PD. Multisubunit DNA-dependent RNA polymerases from vaccinia virus and other nucleocytoplasmic large-DNA viruses: impressions from the age of structure. Microbiol Mol Biol Rev 2017;81. https://doi.org/10.1128/MMBR.00010-17
[11] De Clercq E, Li G. Approved antiviral drugs over the past 50 years. Clin Microbiol Rev 2016;29:695–747. https://doi.org/10.1128/CMR.00102-15
[12] Vora SB, Brothers AW, Englund JA. Renal toxicity in pediatric patients receiving cidofovir for the treatment of adenovirus infection. J Pediatr Infect Dis Soc 2017;6:399–402. https://doi.org/10.1093/JPIDS/PIX011
[13] Sorokina M, Merseburger P, Rajan K, Yirik MA, Steinbeck C. COCONUT online: collection of open natural products database. J Chemin 2021;13:1–13. https://doi.org/10.1186/S13321-020-00478-9
[14] Abduljalil JM, Elfiky AA. Repurposing antiviral drugs against the human monkeypox virus DNA-dependent RNA polymerase; in silico perspective. J Infect 2022;85(6):702–69. https://doi.org/10.1016/j.jinf.2022.09.002
[15] Davis IW, Leaver-Fay A, Chen VB, Block JN, Kapral GJ, Wang X, et al. MolProbity: all-atom contacts and structure validation for proteins and nucleic acids. Nucleic Acids Res 2007;35:W375–83. https://doi.org/10.1093/nar/gkm216
[16] Shapovalov MV, Dunbrack RL. A smoothed backbone-dependent rotamer library for proteins derived from adaptive kernel density estimates and regressions. Structure 2011;19:844–58. https://doi.org/10.1016/J.STR.2011.03.019
[17] Pettersen EF, Goddard TD, Huang CC, Couch GS, Greenblatt DM, Meng EC, et al. UCSF Chimera – a visualization system for exploratory research and analysis. J Comput Chem 2004;25:1605–12. https://doi.org/10.1002/JCC.20084
[18] Abraham MJ, Murtola T, Schulz R, Páll S, Smith JC, Hess B, et al. GROMACS: high performance molecular simulations through multi-level parallelism from laptops to supercomputers. SoftwareX 2015;1–2:19–25. https://doi.org/10.1016/j.softx.2015.06.001
[19] Lee J, Cheng X, Swails JM, Yeom MS, Eastman PK, Lemkul JA, et al. CHARMM-GUI input generator for NAMD, GROMACS, AMBER, OpenMM, and CHARMM/OpenMM simulations using the CHARMM36 additive force field. J Chem Theory Comput 2016;12:405–13. https://doi.org/10.1021/acs.jctc.5b00935
[20] Berendsen HJC, Postma JPM, Van Gunsteren WF, Dinola A, Haak JR. Molecular dynamics with coupling to an external bath. J Chem Phys 1998;81:3684. https://doi.org/10.1063/1.448118
[21] Bussi G, Donadio D, Parrinello M. Canonical sampling through velocity rescaling. J Chem Phys 2007;126:014101. https://doi.org/10.1063/1.2408420
[22] Parrinello M, Rahman A. Polymorphic transitions in single crystals: a new molecular dynamics method. J Appl Phys 1998;52:7182. https://doi.org/10.1063/1.328693
[23] Tubiana T, Carvaillo J-C, Boulard Y, Bressanelli S. TTClust: a versatile molecular simulation trajectory clustering program with graphical summaries. J Chem Inf Model 2018;58:2178–82. https://doi.org/10.1021/ACS.JCIM.8B00512
[24] Gordon JC, Myers JB, Folta T, Shoja V, Heath LS, Onufriev AH. ++: a server for estimating p Ka s and adding missing hydrogens to macromolecules. Nucleic Acids Res 2005;33:W368–71. https://doi.org/10.1093/NAR/GKI464
[25] Morris GM, Huey R, Lindstrom W, Sanner MF, Belew RK, Goodsell DS, et al. AutoDock4 and AutoDockTools4: automated docking with selective receptor flexibility. J Comput Chem 2009;30:2785–91. https://doi.org/10.1002/jcc.21256
[26] Huang K, Fu T, Glass LM, Zitnik M, Xiao C, Sun J. DeepPurpose: a deep learning library for drug–target interaction prediction. Bioinformatics 2021;36:5545–7. https://doi.org/10.1093/bioinformatics/btaa1005
[27] Landrum G. RDKit: Open-source cheminformatics 2006. https://github.com/rdkit/rdkit.
[28] O'Boyle NM, Banck M, James CA, Morley C, Vandermeersch T, Hutchison GR. Open Babel: An Open chemical toolbox. J Chemin- 2011;3:1–14. https://doi.org/10.1186/1758-2946-3-33
[29] Eberhardt J, Santos-Martins D, Tillack AF, Forli S. AutoDock Vina 1.2.0: new docking methods, expanded force field, and python bindings. J Chem Inf Model 2021;61:3891–8. https://doi.org/10.1021/acs.jcim.1c00203
[30] Meng X-Y, Zhang H-X, Mezei M, Cui M. Molecular docking: a powerful approach for structure-based drug discovery. Curr Comput Aided-Drug Des 2012;7:146–57. https://doi.org/10.2174/157340911795677602
[31] Vanommeslaeghe K, Hatcher E, Acharya C, Kundu S, Zhong S, Shim J, et al. CHARMM general force field: a force field for drug-like molecules compatible with the CHARMM all-atom additive biological force fields. J Comput Chem 2010;31:671–90. https://doi.org/10.1002/jcc.21367
[32] Valdés-Tresanco MS, Valdés-Tresanco ME, Valiente PA, Moreno E. Gmx_MMPBSA: a new tool to perform end-state free energy calculations with GROMACS. J Chem Theory Comput 2021;17:6281–91. https://doi.org/10.1021/acs.jctc.1c00645
[33] Wang E, Sun H, Wang J, Wang Z, Liu H, Zhang JZH, et al. End-point binding free energy calculation with MM/PBSA and MM/GBSA: strategies and applications in drug design. Chem Rev 2019;119:9478–508. https://doi.org/10.1021/acs.chemrev.9b00055
[34] Onufriev A, Bashford D, Case DA. Exploring protein native states and large-scale conformational changes with a modified generalized born model. Proteins Struct Funct Bioinforma 2004;55:383–94. https://doi.org/10.1002/PROT.20033
[35] Miller BR, McGee TD, Swails JM, Homeyer N, Gohlke H, Roitberg AE. MMPBSA.py: an efficient program for end-state free energy calculations. J Chem Theory Comput 2012;8:3314–21. https://doi.org/10.1021/ct300418h
[36] Grimm C, Bartuli J, Boettcher B, Szalay AA, Fischer U. Structural basis of the complete poxvirus transcription initiation process. Nat Struct Mol Biol 2021;28:779–88. https://doi.org/10.1038/s41594-021-00655-w
[37] Hillen HS, Bartuli J, Grimm C, Dienemann C, Bedenk K, Szalay AA, et al. Structural basis of poxvirus transcription: transcribing and capping vaccinia complexes. Cell 2019;179:1525–36. https://doi.org/10.1016/j.cell.2019.11.023
[38] Son M, Lee M, Sung GH, Lee T, Shin YS, Cho H, et al. Bioactive activities of natural products against herpesvirus infection. J Microbiol 2013;51:545–51. https://doi.org/10.1007/s12275-013-3450-9
[39] Cao S, Realegeno S, Pant A, Satheshkumar PS, Yang Z. Suppression of poxvirus replication by resveratrol. Front Microbiol 2017;8:2196. https://doi.org/10.3389/FMICB.2017.02196
[40] Abduljalil JM, AL-Rakhami AA, AL-Haj TM, AL-Rrimy AM, Al-Wheabi AS. Preliminary phytochemical analysis and antibacterial activity of methanol extracts from Origanum majorana, Rumex nervosus, and Withania somnifera. Int J Pharma Res Health Sci 2018;6:2844–50.
[41] Samadi AK. Potential Anticancer Properties and Mechanisms of Action of Withanolides. Enzyme 37. Academic Press,; 2015. p. 73–94. https://doi.org/10.1016/BS.ENZ.2015.05.002
[42] Tettamanzi MC, Veleiro AS, De la Fuente JR, Burton G. Withanolides from Salpichroa origanifolia. J Nat Prod 2001;64:783–6. https://doi.org/10.1021/np010010t
[43] Ekiert H, Knut E, Świątkowska J, Klin P, Rzepiela A, Tomczyk M, et al. Artemisia abrotanum L. (Southern Wormwood) — history, current knowledge on the chemistry, biological activity, traditional use and possible new pharmaceutical and cosmetological applications. Molecules 2021;26:2503. https://doi.org/10.3390/MOLECULES26092503